Enhancement of Local Pairing Correlations in Periodically Driven Mott Insulators

Francesco Peronaci,[1, 2, 3, *] Olivier Parcollet,[1, 4] and Marco Schiró[1]

[1] *Institut de Physique Théorique (IPhT), CEA, CNRS, UMR 3681, 91191 Gif-sur-Yvette, France*
[2] *CPHT, Ecole Polytechnique, CNRS, Université Paris-Saclay, 91128 Palaiseau, France*
[3] *Max Planck Institute for the Physics of Complex Systems, Dresden 01187, Germany*
[4] *Center for Computational Quantum Physics, Flatiron Institute, 162 Fifth Avenue, New York, NY 10010, USA*

(Dated: April 2, 2019)

We investigate a model for a Mott insulator in presence of a time-periodic modulated interaction and a coupling to a thermal reservoir. The combination of drive and dissipation leads to non-equilibrium steady states with a large number of doublon excitations, well above the maximum thermal-equilibrium value. We interpret this effect as an enhancement of local pairing correlations, providing analytical arguments based on an effective Floquet Hamiltonian. Strikingly, this effective Hamiltonian shows a tendency to develop long-range staggered superconducting correlations. This suggests the intriguing possibility of realizing the elusive eta-pairing phase of the repulsive Hubbard model in driven-dissipative Mott Insulators.

arXiv:1904.00857v1 [cond-mat.str-el] 1 Apr 2019

The Floquet engineering of complex quantum systems is a very active line of research in today's condensed matter physics [1]. It consists in the design of periodic perturbations to achieve non-equilibrium *driven* states remarkably different from their *undriven* counterparts. Examples are the dynamical control of band topology [2, 3] and of magnetic interactions [4] in ultracold atoms in optical lattices, and of effective Hamiltonian parameters in solids under intense laser-pulse excitation [5, 6].

A useful description of a periodically driven quantum system is in terms of effective static Hamiltonians derived by means of large-frequency expansions [7, 8]. In general, however, the drive affects also the distribution function of the system, eventually leading to thermalization to a trivial infinite-temperature state [9, 10]. Nevertheless, when heating can be avoided for finite but long times, interesting prethermal Floquet states can be observed. This is the case, for example, for very large drive frequency [11–13] or systems close to integrability [14–19]. In particular, Ref. [20] showed that strong electronic correlations lead to finite-frequency prethermal states with remarkable properties as a function of drive frequency.

A natural question concerning the Floquet prethermal state is whether the coupling to external reservoirs would cancel out its interesting features, or rather preserve them and possibly make them more accessible. Particularly interesting is the possibility to control the distribution function of the system by means of a dissipation mechanism of the energy injected by the drive [21–25].

To investigate this point, in this Letter we consider the Fermi-Hubbard model with a periodically driven interaction and coupled to a thermal reservoir. Starting from the large-interaction Mott-insulating phase, our numerical calculations show that the combination of drive and dissipation stabilizes the Floquet prethermal states, leading to steady states that are not accessible in the corresponding isolated model. In particular, we reveal a regime with a remarkably large number of high-energy doublon excitations, well above the maximum equilibrium value for the half-filled repulsive Hubbard model. Crucial to the stability of this regime is that the dissipative bath does not open new channels for doublon decay.

We interpret the steady-state large double occupancy as an enhancement of local pairing correlations, and we describe this effect as a thermalization to a lowest-order Floquet Hamiltonian. Remarkably, we find that higher-order terms can stabilize finite-momentum doublon superfluidity, namely staggered long-range pairing correlations among fermions, which spontaneously break the hidden $\mathrm{SU_C}(2)$ charge symmetry of the half-filled Hubbard model [26–28]. This suggests a nonequilibrium protocol for Floquet engineering exotic superconducting states in driven-dissipative Mott insulators.

These results are relevant for current experiments on laser-pumped organic Mott insulators [6] and on ultracold Fermi gases in driven optical lattices [29, 30]. We discuss the latter in particular, suggesting to explore a possibly overlooked regime in future experiments.

Model – The Hamiltonian of the driven-dissipative Fermi-Hubbard model reads $H = H_{\mathrm{Hub}} + H_{\mathrm{diss}}$, where:

$$H_{\mathrm{Hub}} = \sum_{ij,\sigma} V_{ij} c^\dagger_{i\sigma} c_{j\sigma} + U(t) \sum_i (n_{i\uparrow} - \tfrac{1}{2})(n_{i\downarrow} - \tfrac{1}{2}), \quad (1)$$

$$H_{\mathrm{diss}} = \sum_{i\alpha} \omega_\alpha b^\dagger_{i\alpha} b_{i\alpha} + \lambda \sum_{i\alpha} g_\alpha (n_i - 1)(b_{i\alpha} + b^\dagger_{i\alpha}). \quad (2)$$

Here the c's operators describe fermions hopping with amplitude V_{ij} and subject to a driven local interaction $U(t \geq 0) = U_0 + \delta U \sin \Omega t$. The bare density of states is semicircular with bandwidth $4V$ and we measure energy, frequency and inverse of time ($\hbar = 1$) in units of V. The thermal bath is implemented by independent sets of bosonic modes b's which couple to density at each lattice site, with spectral function $J(\omega) = \sum_\alpha g^2_\alpha \delta(\omega - \omega_\alpha) = \omega^2 e^{-\frac{\omega}{\omega_c}}$ ($\omega_c = 1$) and coupling λ. Importantly, the bath allows energy dissipation but commutes with the density $n_i = n_{i\uparrow} + n_{i\downarrow}$ and preserves particle-hole symmetry. The system remains half filled at all times ($\langle n_{i\sigma} \rangle = 0.5$).

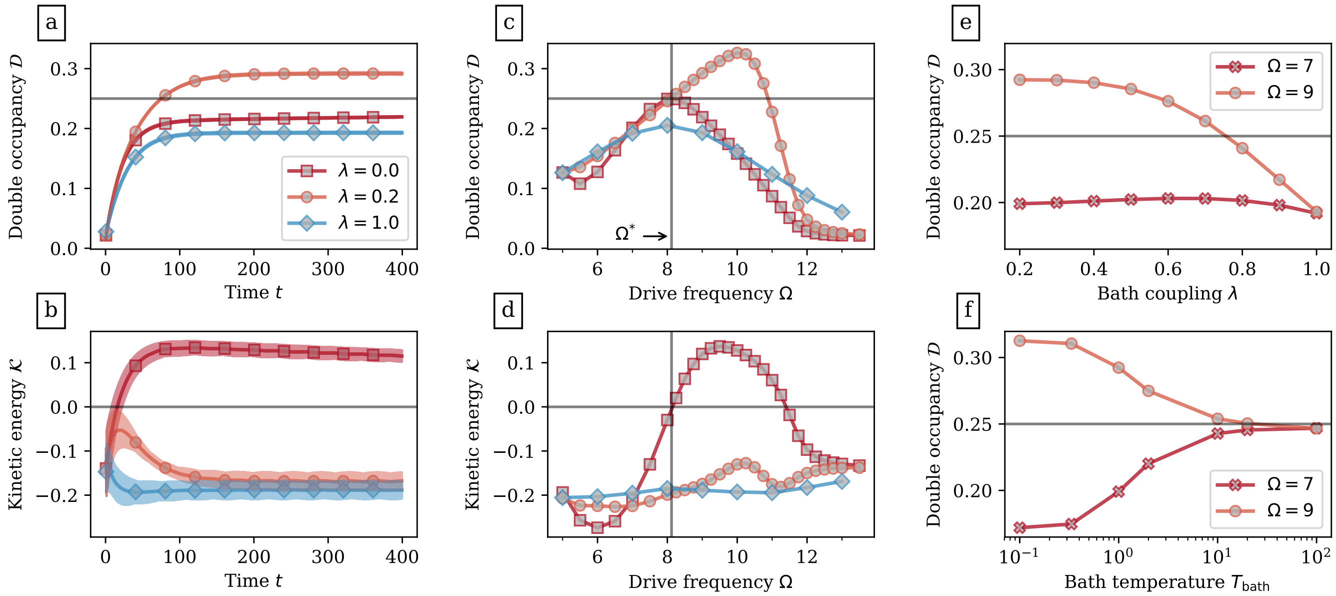

FIG. 1. Panels (a-b): Time evolution of double occupancy and kinetic energy for drive frequency $\Omega = 9 > \Omega^*$: fast oscillations (shaded area) and their average (symbols). Legend in (a) is common to (a-b-c-d). Panels (c-d): Long-time average of double occupancy and kinetic energy as a function of drive frequency. Panels (e-f): Long-time average of double occupancy as a function of bath coupling and of bath temperature for $\lambda = 0.2$ and drive frequencies $\Omega = 7 < \Omega^*$ and $\Omega = 9 > \Omega^*$.

Starting from a thermal state at temperature T, we calculate the time evolution within nonequilibrium dynamical mean-field theory [31, 32] with the non-crossing-approximation impurity solver [33, 34]. This is appropriately modified [35] to include the effect of dissipation at order $\mathcal{O}(\lambda^2)$ (see Supplemental Material [36] Sec. I for implementation details, and Sec. II for benchmarks with the one-crossing-approximation). We calculate the double occupancy $\mathcal{D}(t) = \langle n_{i\uparrow}(t) n_{i\downarrow}(t)\rangle$, the kinetic energy $\mathcal{K}(t) = \sum V_{ij} \langle c^\dagger_{i\sigma}(t) c_{j\sigma}(t)\rangle$, and the local Green's function $G_\sigma(t,t') = -i\,\langle \mathrm{T} c_{i\sigma}(t) c^\dagger_{i\sigma}(t')\rangle$. For definiteness, we choose $U_0 = 8$ and $T = 1$ for the initial Mott-insulating state, $\delta U = 2$ for the drive amplitude. The bath temperature is $T_{\mathrm{bath}} = 1$ unless specified differently. In absence of dissipation, Floquet prethermalization is observed at all frequencies except the resonance $\Omega^* = 8.12 \simeq U_0$ [20].

Time evolution – In the driven-dissipative model, as well as in the isolated case, double occupancy and kinetic energy display a separation of time scales between fast oscillations synchronized with the drive and a slowly varying average value. However, after a common transient, the thermal reservoir starts to be effective and has dramatic effects on both observables.

For weak bath coupling and drive above resonance, the double occupancy grows substantially larger than in the isolated model, going to a stationary average above 0.25 (Fig. 1a; $\lambda = 0.2$). Such a large value would be possible, at equilibrium, only if the interaction were *attractive*. This striking effect highlights the peculiarity of this non-equilibrium steady state, as we discuss thoroughly below.

Upon increasing the bath coupling (Fig. 1a; $\lambda = 1.0$), the double occupancy decreases and eventually remains below the limit of 0.25 at all times. Moreover, we notice that the bath is effective only after a transient time $\sim 1/\lambda^2$, which makes the regime of very weak coupling not accessible by the numerical simulation (see also Ref. [37]).

At the same time, the kinetic energy is also largely affected by dissipation (Fig. 1b). Here the effect is more intuitive: in the isolated model the drive leads to a prethermal state with positive kinetic energy, indicative of a population inversion [18, 20]. On the other hand, the thermal reservoir dissipates the excess kinetic energy, which remains negative as at equilibrium, and inhibits the population inversion, as we also explicitly show below.

Long-time average – To study the role of drive frequency and bath coupling in a more systematic way, we consider the long-time average of double occupancy and kinetic energy. For weak bath coupling, the dissipative model has double occupancy larger than the isolated one at all frequencies (Fig. 1c; $\lambda = 0.2$). However, a remarkable change happens crossing the resonance $\Omega^* \simeq U_0$. Below resonance, the dissipation has only a quantitative, rather weak effect. In contrast, above resonance, we systematically observe a large increase of double occupancy across the limit of 0.25, as discussed previously for a selected frequency. Lower values are then recovered upon increasing the frequency further, as the system eventually becomes transparent to the drive.

Independent of the bath coupling, the kinetic energy of the dissipative model is rather featureless and negative

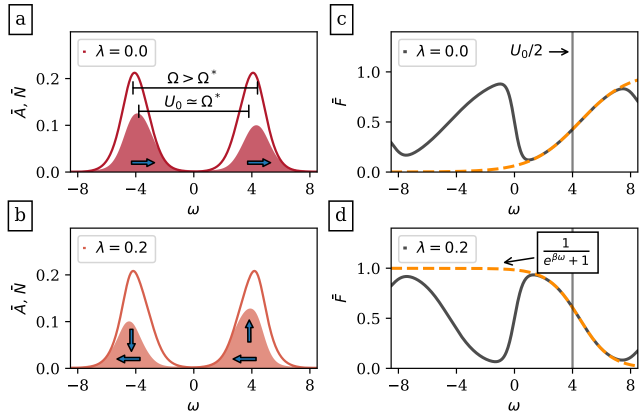

FIG. 2. Panels (a-b): Long-time average spectral function $\bar{A}(\omega)$ (solid line) and occupation function $\bar{N}(\omega)$ (filled area) of the isolated model ($\lambda = 0$) and the dissipative model ($\lambda = 0.2$) for drive frequency $\Omega = 9 > \Omega^*$. The isolated model (a) has population inversion, signaled by the blueshift of $\bar{N}(\omega)$ with respect to $\bar{A}(\omega)$ (arrows). In the dissipative model (b), the thermal reservoir cancels the population inversion (horizontal arrows) and unveils a non-thermal state with large double occupancy, signaled by the increase of $\bar{N}(\omega)$ in the high-energy band (vertical arrows). Panels (c-d): Long-time average distribution function $\bar{F}(\omega)$ for the same parameters of (a-b) with Fermi-function fit around the Hubbard-band center. The extracted effective temperature is $T_{\text{eff}} = -1.6$ for the isolated model (c) and $T_{\text{eff}} = 1.1 \simeq T_{\text{bath}}$ for the dissipative one (d). See Supplemental Material [36] Fig. S3 for a plot of $T_{\text{eff}}(\Omega)$.

for all frequencies (Fig. 1d; $\lambda = 0.2, 1.0$). Thus, the thermal reservoir cancels the region of positive kinetic energy characteristic of the isolated case (Fig. 1d; $\lambda = 0.0$).

The difference between below and above resonance appears also in the dependence on bath coupling (Fig. 1e) and on bath temperature (Fig. 1f). Below resonance ($\Omega = 7$) there is almost no dependence on bath coupling and double occupancy decreases upon lowering the bath temperature. Quite differently, above resonance ($\Omega = 9$) the double occupancy increases for weak bath coupling, and upon decreasing the bath temperature.

We notice that the observed behavior depends strongly on the bosonic nature of the dissipative bath. Indeed a fermionic reservoir would not lead to the same anomalous increase in steady-state double occupancy, as we show in Sec. III of Supplemental Material [36].

Spectral function – To gain insight into the nature of the steady state, we calculate the spectral function $\bar{A}(\omega)$ and occupation function $\bar{N}(\omega)$ as the average Wigner transforms of the retarded and lesser components of the local Green's function [20]. While the spectral function is the same in the isolated and dissipative models, the occupation function, and thus the distribution function $\bar{F}(\omega) = \bar{N}(\omega)/\bar{A}(\omega)$, changes drastically for drive frequency above resonance and weak bath coupling.

In the isolated model, $\bar{N}(\omega)$ is shifted towards high energy with respect to $\bar{A}(\omega)$ (Fig. 2a). There is therefore a population inversion within the Hubbard bands. Indeed, the local behavior of $\bar{F}(\omega)$ for $\omega \simeq \pm U_0/2$ has the shape of a Fermi function with negative temperature (Fig. 2c).

The thermal reservoir completely changes the situation. First, as the dissipation enhances the energy redistribution within the Hubbard bands, $\bar{N}(\omega)$ is pushed back to lower energy (Fig. 2b), cancelling the population inversion. As a consequence, $\bar{F}(\omega)$ assumes the shape of a Fermi function with positive temperature for $\omega \simeq \pm U_0/2$ (Fig. 2d). Then, the overall weight of $\bar{N}(\omega)$ in the upper band grows and becomes even larger than in the lower band, meaning the creation of a large number of high-energy doublon excitations. These two effects are qualitatively related to the ones discussed above: change of sign of kinetic energy and growth of double occupancy.

Discussion – The above numerical results demonstrate that, in the strongly repulsive Fermi-Hubbard model, the combination of a time-periodic interaction and a dissipative bath leads to steady states with a remarkably large number of doublon excitations. Interestingly, this large double occupancy immediately translates into enhanced local pairing correlations $\mathcal{D} = \langle c^\dagger_{i\uparrow} c^\dagger_{i\downarrow} c_{j\downarrow} c_{j\uparrow} \rangle |_{i=j}$.

In order to unveil the origin of this effect, we consider a frequency close to resonance $\Omega \simeq \Omega^* \simeq U_0$ and perform a rotating-frame transformation on the Hamiltonian (1) followed by a high-frequency expansion [38] (see Supplemental Material [36] Sec. V). At lowest order, we find a correlated hopping term and a frequency-dependent local interaction:

$$\bar{H}^{\text{eff}(0)}_{\text{Hub}} = VK_0 + (U_0 - \Omega) \sum\nolimits_i (n_{i\uparrow} - \tfrac{1}{2})(n_{i\downarrow} - \tfrac{1}{2}). \quad (3)$$

Here $K_0 = \sum (V_{ij}/V) c^\dagger_{i\sigma} c_{j\sigma} (n_{i\bar{\sigma}} n_{j\bar{\sigma}} + \bar{n}_{i\bar{\sigma}} \bar{n}_{j\bar{\sigma}})$ are those hopping terms in Eq. (1) that do not alter the number of doubly occupied sites ($\bar{n}_{i\sigma} = 1 - n_{i\sigma}$, $\bar{\uparrow} = \downarrow$ and $\bar{\downarrow} = \uparrow$). The effective Hamiltonian (3) conserves the total double occupancy, and controls its long-time value in both the isolated and the dissipative model. To see this, we extract the effective temperature from the numerical results, obtaining $T_{\text{eff}}(\Omega) \propto (U_0 - \Omega)^{-1}$ for the isolated model and $T_{\text{eff}} \simeq T_{\text{bath}}$ for the dissipative one (see Supplemental Material [36] Fig. S3). Then, since $|T_{\text{eff}}| \gtrsim V$, we can disregard the kinetic term in Eq. (3) and estimate $\mathcal{D} = 0.5[1+\exp(0.5(U_0-\Omega)/T_{\text{eff}})]^{-1}$. For frequency close to resonance $\Omega \simeq U_0$, this gives quadratic behavior $\mathcal{D} - 0.25 \propto -(\Omega - U_0)^2$ in the isolated model, and linear dependence $\mathcal{D} - 0.25 \propto (\Omega - U_0)$ in the dissipative model, qualitatively reproducing the results in Fig. 1c.

In other words, we interpret the long-time value of double occupancy as the thermal value of the Floquet Hamiltonian (3), where the second term promotes large double occupancy for $\Omega > U_0$. In the isolated model, this effect is counterbalanced by the concomitant population inversion (see also Ref. [18]), whereas in the dissipative model the thermal reservoir inhibits the population inversion, allows the increase of double occupancy and, crucially, turns the Floquet prethermal state in a true steady state.

Incidentally, we notice that strong correlations persist even for $\Omega \simeq U_0$, as shown by the large Mott gap. This fundamentally differs from the case of dynamical band flipping [39] where, moreover, the large double occupancy is transient and triggered by population inversion and, thus, it is completely different from what discussed here.

A natural question, at this point, is whether the enhanced local pairing correlations can propagate through the lattice, giving rise to a superfluid state of doublons. To answer this, we consider the next-order terms in the Floquet Hamiltonian [36]:

$$\bar{H}^{\mathrm{eff}(1)}_{\mathrm{Hub}} = (-i\mathcal{J}_1(\tfrac{\delta U}{\Omega})VK_+ + \mathrm{H.c.}) + \tfrac{V^2}{\Omega}(\mathcal{J}_0(\tfrac{\delta U}{\Omega}))^2[K_+, K_-]. \tag{4}$$

Here $\mathcal{J}_n(x)$ is the n-th order Bessel function of the first kind, $K_+ = \sum(V_{ij}/V)c^\dagger_{i\sigma}c_{j\sigma}n_{i\bar{\sigma}}\bar{n}_{j\bar{\sigma}} = (K_-)^\dagger$ and one has to note that, in the case of weak drive amplitude considered here, $\mathcal{J}_n(\delta U/\Omega) \sim (\delta U/\Omega)^n$ and therefore all terms in Eq. (4) indeed vanish as the inverse drive frequency.

The first two terms in Eq. (4) create or annihilate doublon excitations, controlling the transient from the initial state to the steady state with large double occupancy. However, these processes are largely inhibited in the steady state. Indeed, only these terms are sensitive to δU and numerical calculations [20] shows how the drive amplitude controls the transient time-scale, but does not influence the long-time steady-state values.

Finally, the last term in Eq. (4) is similar to the Schrieffer-Wolff result [40] and at equilibrium ($\delta U = 0$) this gives the usual anti-ferromagnetic Heisenberg model. Out of equilibrium, as pointed out in Ref. [41], states with large double occupancy become relevant, and the same term leads to completely different physics. This is precisely our case, where a large non-equilibrium doublon population is stabilized by drive and dissipation.

Indeed, in the limit of double occupancy so large that singly occupied sites can be neglected, we can rewrite the Floquet Hamiltonian in terms of the doublons only [36]:

$$\bar{H}^{\mathrm{eff}}_{\mathrm{Hub}} = J_{\mathrm{eff}} \sum\nolimits_{\langle ij\rangle} (c^\dagger_{i\uparrow}c^\dagger_{i\downarrow}c_{j\downarrow}c_{j\uparrow} + n_{i\uparrow}n_{i\downarrow}\bar{n}_{j\uparrow}\bar{n}_{j\downarrow}). \tag{5}$$

Here $J_{\mathrm{eff}} = 2V^2/\Omega(\mathcal{J}_0(\delta U/\Omega))^2$, the first term is a doublon hopping, and the second term is a first-neighbor doublon interaction. The physics encoded in the Hamiltonian (5) is best discussed by means of a transformation on the spin down only $c_{i\downarrow} \to \tilde{c}_{i\downarrow} = (-1)^i c^\dagger_{i\downarrow}$ which recast Eq. (5) in the form of an isotropic ferromagnetic Heisenberg model $\bar{H}^{\mathrm{eff}}_{\mathrm{Hub}} = -J_{\mathrm{eff}} \sum \boldsymbol{\eta}_i \cdot \boldsymbol{\eta}_j$ for the so-called η-spins: $\boldsymbol{\eta}_i = \frac{1}{2}\sum_{\alpha\beta} \tilde{c}^\dagger_{i\alpha}\boldsymbol{\sigma}_{\alpha\beta}\tilde{c}_{i\beta}$ [36]. The invariance under η-spin rotation is then associated to the charge-$\mathrm{SU_C}(2)$ invariance of the Hamiltonian (1) under rotation of the doublon-holon doublet $\{|0\rangle, |\uparrow\downarrow\rangle\}$ [41]. Remarkably, this can be used to build eigenstates with staggered long-range superconducting correlations (η-pairing) [26, 27]. These are precisely the pairing correlations encoded in the Hamiltonian (5). Indeed, the η-spin Heisenberg ferromagnetic model has a magnetization $\langle \eta^z \rangle = \mathcal{D} - 0.5$ fixed by the double occupancy and, below a critical temperature $T_c \sim J_{\mathrm{eff}}$, develops a finite order parameter in the xy plane which corresponds to staggered long-range pairing correlations $\langle c^\dagger_{i\uparrow}c^\dagger_{i\downarrow} + \mathrm{H.c.}\rangle = (-1)^i \langle 2\eta^x_i \rangle = (-1)^i\sqrt{4\mathcal{D}(1-\mathcal{D})}$. We notice, however, that the $\mathrm{SU_C}(2)$ symmetry implies a degeneracy between the xy-plane and the z-axis of the η-spin, which translates into a competition between superfluidity and charge-density wave in Eq. (5). The investigation of such broken-symmetry phases is beyond the scope of this Letter and is left for future work.

The model system investigated here can be realized in current experimental platforms. Particularly promising are Mott-insulating organic molecular crystals, where it was shown that intense laser excitations can effectively act as a time-periodic modulation of the interaction [6]. A more direct control is achieved with ultracold atoms in optical lattices. Recent experiments [29, 30] have studied the Floquet prethermal time scales and, remarkably, have found large double occupancy for drive above resonance. Here we suggest that, also in this case, a key role is played by dissipation, which is unavoidable even in cold atoms. Finally, we notice that these experiments have focused on the regime where the correlated kinetic term simplifies to give a renormalized Hubbard model. In contrast, here we have studied the case of a Floquet Hamiltonian for the doublon excitations only. Therefore, we suggest future experiments to explore this regime to investigate the presence of staggered pairing correlations, which can be easily detected on these platforms.

Conclusions – In this Letter, we have studied the combined effect of a periodically driven interaction and a dissipative bath in the strongly repulsive Fermi-Hubbard model. Our numerical calculations show that the Floquet prethermal states of the isolated model become steady states of the dissipative model. For weak bath coupling and drive above resonance, these have a stable and very large population of high-energy doublon excitations, which we interpret as enhanced local pairing correlations.

We rationalize this effect as a thermalization of double occupancy to a lowest-order Floquet Hamiltonian. Remarkably, including also higher-order terms, we can write the Hamiltonian which governs the steady state in terms of the doublons only. Here, we find terms which spread the pairing correlations in staggered configuration (η-pairing). Below a frequency-dependent critical temperature, these would induce off-diagonal long-range order, hence a superfluid phase of doublon excitations. Thus, our results suggest a path to Floquet engineering stable exotic superconducting states in driven-dissipative Mott insulators.

Note added – Recently, exact numerical results on finite-size systems have also found evidence of η-pairing in a photo-excited one-dimensional Mott insulator [42].

This work was supported by the European Research Council grants ERC-319286-QMAC (FP) and ERC-278472-MottMetals (FP, OP). The Flatiron Institute is a division of the Simons Foundation. MS acknowledges support from a grant "Investissements d'Avenir" from LabEx PALM (ANR-10-LABX-0039-PALM) and from the CNRS through the PICS-USA-14750.

* fperonaci@pks.mpg.de

[1] T. Oka and S. Kitamura, Annual Review of Condensed Matter Physics **10**, annurev (2018).
[2] T. Oka and H. Aoki, Physical Review B **79**, 081406 (2009).
[3] G. Jotzu, M. Messer, R. Desbuquois, M. Lebrat, T. Uehlinger, D. Greif, and T. Esslinger, Nature **515**, 237 (2014).
[4] F. Görg, M. Messer, K. Sandholzer, G. Jotzu, R. Desbuquois, and T. Esslinger, Nature **553**, 481 (2018).
[5] A. Subedi, A. Cavalleri, and A. Georges, Physical Review B **89**, 220301 (2014).
[6] R. Singla, G. Cotugno, S. Kaiser, M. Först, M. Mitrano, H. Y. Liu, A. Cartella, C. Manzoni, H. Okamoto, T. Hasegawa, S. R. Clark, D. Jaksch, and A. Cavalleri, Physical Review Letters **115**, 187401 (2015).
[7] N. Goldman and J. Dalibard, Physical Review X **4**, 031027 (2014).
[8] M. Bukov, L. D'Alessio, and A. Polkovnikov, Advances in Physics **64**, 139 (2015).
[9] A. Lazarides, A. Das, and R. Moessner, Physical Review Letters **112**, 150401 (2014).
[10] L. D'Alessio and M. Rigol, Physical Review X **4**, 041048 (2014).
[11] D. A. Abanin, W. De Roeck, and F. Huveneers, Physical Review Letters **115**, 256803 (2015).
[12] T. Mori, T. Kuwahara, and K. Saito, Physical Review Letters **116**, 120401 (2016).
[13] D. A. Abanin, W. De Roeck, W. W. Ho, and F. Huveneers, Physical Review B **95**, 014112 (2017).
[14] M. Bukov, S. Gopalakrishnan, M. Knap, and E. Demler, Physical Review Letters **115**, 205301 (2015).
[15] E. Canovi, M. Kollar, and M. Eckstein, Physical Review E **93**, 012130 (2016).
[16] S. A. Weidinger and M. Knap, Scientific Reports **7**, 45382 (2016).
[17] K. Seetharam, P. Titum, M. Kolodrubetz, and G. Refael, Physical Review B **97**, 014311 (2018).
[18] A. Herrmann, Y. Murakami, M. Eckstein, and P. Werner, EPL **120**, 57001 (2018).
[19] Y. Baum, E. P. L. van Nieuwenburg, and G. Refael, SciPost Physics **5**, 017 (2018).
[20] F. Peronaci, M. Schiró, and O. Parcollet, Physical Review Letters **120**, 197601 (2018).
[21] T. Iadecola, D. Campbell, C. Chamon, C. Y. Hou, R. Jackiw, S. Y. Pi, and S. V. Kusminskiy, Physical Review Letters **110**, 176603 (2013).
[22] T. Iadecola, T. Neupert, and C. Chamon, Physical Review B **91**, 235133 (2015).
[23] K. I. Seetharam, C. E. Bardyn, N. H. Lindner, M. S. Rudner, and G. Refael, Physical Review X **5**, 041050 (2015).
[24] K. I. Seetharam, C. E. Bardyn, N. H. Lindner, M. S. Rudner, and G. Refael, Physical Review B **99**, 014307 (2019).
[25] O. Hart, G. Goldstein, C. Chamon, and C. Castelnovo, arXiv:1810.12309 (2018).
[26] C. N. Yang, Physical Review Letters **63**, 2144 (1989).
[27] S. Zhang, Physical Review Letters **65**, 120 (1990).
[28] D. Mitra, P. T. Brown, E. Guardado-Sanchez, S. S. Kondov, T. Devakul, D. A. Huse, P. Schauß, and W. S. Bakr, Nature Physics **14**, 173 (2018).
[29] M. Messer, K. Sandholzer, F. Görg, J. Minguzzi, R. Desbuquois, and T. Esslinger, Physical Review Letters **121**, 233603 (2018).
[30] K. Sandholzer, Y. Murakami, F. Görg, J. Minguzzi, M. Messer, R. Desbuquois, M. Eckstein, P. Werner, and T. Esslinger, arXiv:1811.12826 (2018).
[31] A. Georges, G. Kotliar, W. Krauth, and M. J. Rozenberg, Reviews of Modern Physics **68**, 13 (1996).
[32] H. Aoki, N. Tsuji, M. Eckstein, M. Kollar, T. Oka, and P. Werner, Reviews of Modern Physics **86**, 779 (2014).
[33] M. Eckstein and P. Werner, Physical Review B **82**, 115115 (2010).
[34] A. Rüegg, E. Gull, G. A. Fiete, and A. J. Millis, Physical Review B **87**, 075124 (2013).
[35] H. T. Chen, G. Cohen, A. J. Millis, and D. R. Reichman, Physical Review B **93**, 174309 (2016).
[36] See Supplemental Material at ...
[37] M. Eckstein and P. Werner, Physical Review Letters **110**, 126401 (2013).
[38] M. Bukov, M. Kolodrubetz, and A. Polkovnikov, Physical Review Letters **116**, 125301 (2016).
[39] N. Tsuji, T. Oka, P. Werner, and H. Aoki, Physical Review Letters **106**, 236401 (2011).
[40] A. H. MacDonald, S. M. Girvin, and D. Yoshioka, Physical Review B **37**, 9753 (1988).
[41] A. Rosch, D. Rasch, B. Binz, and M. Vojta, Physical Review Letters **101**, 265301 (2008).
[42] T. Kaneko, T. Shirakawa, S. Sorella, and S. Yunoki, Physical Review Letters **122**, 077002 (2019).

Supplemental Material

I. NCA WITH BOSONIC BATH

Here we describe our implementation of a bosonic bath in the non-crossing-approximation (NCA) impurity solver for non-equilibrium dynamical mean-field theory (DMFT). Starting from Hamiltonians (1) and (2) in main text, we integrate out the bosons and obtain the action:

$$\begin{aligned} S_{\text{latt}} = &\int \mathrm{d}t \sum_{ij,\sigma} V_{ij} c^\dagger_{i\sigma}(t) c_{j\sigma}(t) \\ &+ \int \mathrm{d}t\, U(t) \sum_i (n_{i\uparrow}(t) - \tfrac{1}{2})(n_{i\downarrow}(t) - \tfrac{1}{2}) \\ &+ \lambda^2 \int\int \mathrm{d}t\, \mathrm{d}t'\, \Delta_b(t,t') \sum_i (n_i(t) - 1)(n_i(t') - 1). \end{aligned} \tag{S1}$$

Here the integrals are along the three-branch Keldysh contour and the bath enters via the hybridization $\Delta_b(t,t') = -i\int \mathrm{d}\omega\, J(\omega)(\theta(t,t') + n_B(\omega/T_{\text{bath}}))e^{-i\omega(t-t')}$ where $\theta(t,t')$ is the Heaviside theta function on contour and $n_b(\omega)$ is the Bose distribution.

In DMFT the lattice action (S1) is mapped onto the action of a quantum impurity coupled to a self-consistent fermionic bath:

$$\begin{aligned} S_{\text{imp}} = &\int \mathrm{d}t\, U(t)(n_\uparrow(t) - \tfrac{1}{2})(n_\downarrow(t) - \tfrac{1}{2}) \\ &+ V^2 \int\int \mathrm{d}t\, \mathrm{d}t'\, G(t,t') \sum_\sigma c^\dagger_\sigma(t) c_\sigma(t') \\ &+ \lambda^2 \int\int \mathrm{d}t\, \mathrm{d}t'\, \Delta_b(t,t')(n(t) - 1)(n(t') - 1). \end{aligned} \tag{S2}$$

Here we have used the relation $\Delta(t,t') = V^2 G(t,t')$ for the hybridization $\Delta(t,t')$ of the self-consistent fermionic bath, which is valid on Bethe lattice.

To derive the NCA equations, we expand the partition function $\mathrm{Tr}(\exp[-iS_{\text{imp}}])$ into a power series in V and λ and truncate the expansion at the first self-consistent order [33–35]. This series is expressed in terms of the propagator of the states of the impurity R, and of its self-energy S, which satisfy an integro-differential equation similar to the usual Dyson equation (see Ref. [20] for our implementation). Then, in the present case a convenient basis choice is $\{|0\rangle, |\uparrow\rangle, |\downarrow\rangle, |\uparrow\downarrow\rangle\}$ which makes the propagator R and the self-energy S diagonal. Finally, we exploit the spin SU(2) symmetry and the particle-hole $\mathrm{SU_C}(2)$ symmetry of Eq. (S2) which further reduce the number of propagators to two: one for the empty state $|0\rangle$ and one for the singly-occupied state $|\uparrow\rangle$, with the following self-energies:

$$\begin{aligned} S_{|0\rangle}(t,t') = &-2iR_{|\uparrow\rangle}(t,t')\Delta(t',t) \\ &+ i\lambda^2 R_{|0\rangle}(t,t')(\Delta_b(t,t') + \Delta_b(t',t)), \end{aligned} \tag{S3}$$

$$S_{|\uparrow\rangle}(t,t') = +2iR_{|0\rangle}(t,t')\Delta(t,t'). \tag{S4}$$

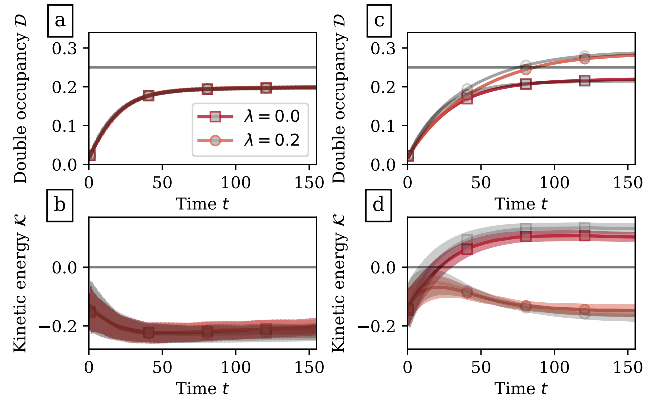

FIG. S1. Time evolution of double occupancy and kinetic energy using the OCA impurity solver for DMFT: Isolated model ($\lambda = 0$) and dissipative model ($\lambda = 0.2$) for drive frequency below resonance $\Omega = 7$ (a-b) and above resonance $\Omega = 9$ (c-d). Legend in (a) is common to (a-b-c-d). Light grey curves are the corresponding NCA results, for comparison.

II. OCA BENCHMARK

In this work we investigate the Mott-insulating phase of the Fermi-Hubbard model with average interaction parameter $U_0 = 8V$ much larger than the bare band-width $W = 4V$. Moreover, we consider initial thermal density matrix at a rather high temperature $T = 1$. In these conditions, the NCA approximation is expected to perform well both at equilibrium and out of equilibrium [33].

To confirm this, we have performed some calculations using the next-order one-crossing approximation (OCA). This takes into consideration terms of order $\mathcal{O}(V^4)$ in the hybridization expansion [33, 34] (see Ref. [20] for our implementation). As expected, the time evolution of double occupancy and kinetic energy (Fig. S1) is essentially identical to the one shown in the main text (Fig. 1a-b).

III. FERMIONIC BATH

It is interesting to consider an external reservoir of fermionic modes, instead of the bosonic bath considered in the main text. To do so, we substitute Eq. (2) of the main text with the following coupling to a fermionic bath:

$$H_{\text{diss}} = \sum_{i\alpha} \omega_\alpha f^\dagger_{i\alpha} f_{i\alpha} + \lambda \sum_{i\sigma\alpha} (g_\alpha c^\dagger_{i\sigma} f_{i\alpha} + g^*_\alpha f^\dagger_{i\alpha} c_{i\sigma}). \tag{S5}$$

Here the operators f's represent sets of independent fermionic harmonic oscillators. In this case, the system can dissipate both energy and particles. Moreover, this type of coupling can be treated exactly: integrating out the fermionic bath, we introduce an additional hybridization $\Delta_f(t,t')$ which can simply be added to the DMFT self-consistent hybridization $\Delta(t,t')$.

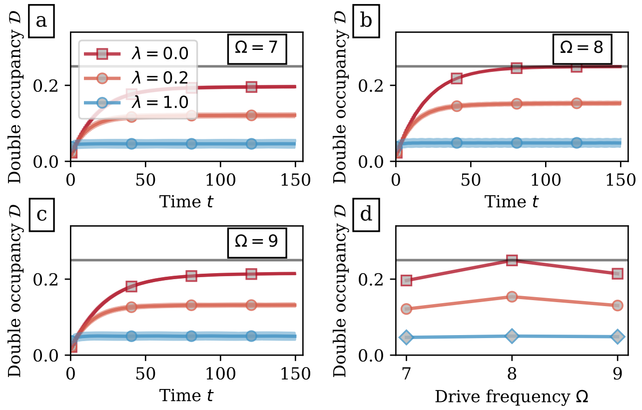

FIG. S2. Panels (a-b-c): Time evolution of double occupancy for the isolated model ($\lambda = 0.0$) and the dissipative one with fermionic bath ($\lambda = 0.2, 1.0$) for various drive frequencies. Legend in (a) is common to (a-b-c-d). Panel (d): Long-time average of double occupancy as a function of drive frequency.

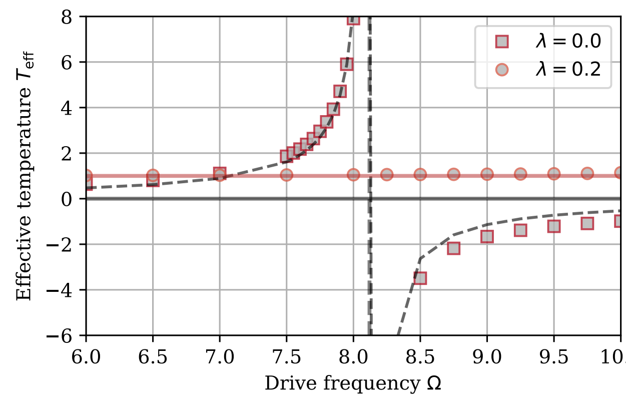

FIG. S3. Effective temperature (symbols) as a function of drive frequency for the isolated model ($\lambda = 0.0$) and the dissipative one ($\lambda = 0.2$). In the former, the effective temperature diverges as $(\Omega^* - \Omega)^{-1}$ (dashed line). The divergence at $\Omega = \Omega^*$ signals the resonant thermalization, while the negative effective temperature for $\Omega > \Omega^*$ signals the population inversion [20]. In contrast, the dissipative model has temperature $\simeq T_{\rm bath}$ (solid line) fixed by the thermal reservoir.

As shown in Fig. S2, the coupling with a fermionic bath does not lead to the same interesting features discussed in the main text for the bosonic bath (cf. Fig. 1a-c). This is due to the fact that the bosonic bath, as opposed to the fermionic bath, commutes with the local density and conserves double occupancy, and therefore it preserves the mechanism for Floquet prethermalization.

IV. EFFECTIVE TEMPERATURE

In Fig. 2 of main text we show the steady-state average distribution function $\bar{F}(\omega)$ for $\Omega = 9 > \Omega^*$, along with a Fermi-function fit $[1+\exp(\omega/T_{\rm eff})]^{-1}$ around the center of the upper Hubbard band $\omega \simeq U_0/2$. From this fit we can extract the effective temperature $T_{\rm eff}$. Here, in Fig. S2 we plot this effective temperature for the isolated and the dissipative models, as a function of the drive frequency.

V. ROTATING-FRAME TRANSFORMATION AND HIGH-FREQUENCY EXPANSION

To carry out the large-frequency expansion [8, 38], we first need to transform Hamiltonian (1) of main text to a rotating frame with respect to the interaction:

$$H_{\rm Hub}(t) = \sum V_{ij} c^\dagger_{i\sigma} c_{j\sigma} + U(t) \sum\nolimits_i (n_{i\uparrow} - \tfrac{1}{2})(n_{i\downarrow} - \tfrac{1}{2}), \tag{S6}$$

$$\bar{H}_{\rm Hub}(t) = e^{S(t)} (H_{\rm Hub}(t) - i\partial_t) e^{-S(t)}, \tag{S7}$$

$$S(t) = iF(t) \sum\nolimits_i (n_{i\uparrow} - \tfrac{1}{2})(n_{i\downarrow} - \tfrac{1}{2}), \tag{S8}$$

$$F(t) = \Omega t - (\delta U/\Omega) \cos \Omega t. \tag{S9}$$

It is useful to introduce the operators K_0 and $K_\pm$ as in the main text ($\bar{n}_{i\sigma} = 1 - n_{i\sigma}$, $\bar{\uparrow} = \downarrow$ and $\bar{\downarrow} = \uparrow$):

$$K_0 = \sum\nolimits_{ij\sigma} (V_{ij}/V) c^\dagger_{i\sigma} c_{j\sigma} (n_{i\bar{\sigma}} n_{j\bar{\sigma}} + \bar{n}_{i\bar{\sigma}} \bar{n}_{j\bar{\sigma}}), \tag{S10}$$

$$K_+ = \sum\nolimits_{ij\sigma} (V_{ij}/V) c^\dagger_{i\sigma} c_{j\sigma} n_{i\bar{\sigma}} \bar{n}_{j\bar{\sigma}} = (K_-)^\dagger. \tag{S11}$$

It is easy to verify that $\sum V_{ij} c^\dagger_{i\sigma} c_{j\sigma} = V(K_0 + K_+ + K_-)$. Then, using $[D, K_0] = 0$ and $[D, K_+] = \pm K_\pm$ we find:

$$\begin{aligned} \bar{H}_{\rm Hub}(t) = {} & V(K_0 + e^{iF(t)} K_+ + e^{-iF(t)} K_-) \\ & + (U_0 - \Omega) \sum\nolimits_i (n_{i\uparrow} - \tfrac{1}{2})(n_{i\downarrow} - \tfrac{1}{2}). \end{aligned} \tag{S12}$$

The rotated Hamiltonian maintains the $2\pi/\Omega$-periodicity. Its Fourier components contain the Bessel function of the first kind $\int_0^{2\pi} {\rm d}\tau \, \exp(i(x\cos\tau - m\tau)) = 2\pi i^m \mathcal{J}_m(x)$ through the following expansions:

$$e^{iF(t)} = \sum\nolimits_m (-i)^{1+m} \mathcal{J}_{1+m}(\tfrac{\delta U}{\Omega}) e^{-im\Omega t}, \tag{S13}$$

$$e^{-iF(t)} = \sum\nolimits_m i^{1-m} \mathcal{J}_{1-m}(\tfrac{\delta U}{\Omega}) e^{-im\Omega t}. \tag{S14}$$

In particular, the average Hamiltonian and the first Fourier components read:

$$\begin{aligned} \bar{H}^{(0)}_{\rm Hub} = {} & VK_0 - i\mathcal{J}_1(\tfrac{\delta U}{\Omega}) VK_+ + i\mathcal{J}_1(\tfrac{\delta U}{\Omega}) VK_- \\ & + (U_0 - \Omega) \sum\nolimits_i (n_{i\uparrow} - \tfrac{1}{2})(n_{i\downarrow} - \tfrac{1}{2}), \end{aligned} \tag{S15a}$$

$$\bar{H}^{(1)}_{\rm Hub} = -\mathcal{J}_2(\tfrac{\delta U}{\Omega}) VK_+ + \mathcal{J}_0(\tfrac{\delta U}{\Omega}) VK_-, \tag{S15b}$$

$$\bar{H}^{(-1)}_{\rm Hub} = \mathcal{J}_0(\tfrac{\delta U}{\Omega}) VK_+ - \mathcal{J}_2(\tfrac{\delta U}{\Omega}) VK_-. \tag{S15c}$$

Eqs. (3) and (4) of main text

Here we calculate the first two terms of the (van-Vleck) large-frequency expansion, with general expression [38]:

$$H_F = H_0 + \sum_{m>0} \frac{[H_{-m}, H_m]}{m\Omega} + \mathcal{O}(\tfrac{1}{\Omega^2}). \tag{S16}$$

The Fourier components H_m are given in Eqs. (S15) and depend on frequency through the Bessel function. When the large-frequency limit is taken at fixed $\delta U/\Omega$, this dependence does not show up in the expansion. In contrast, here we keep δU constant and we have to consider the asymptotic behavior $\mathcal{J}_n(\delta U/\Omega) \sim (\delta U/\Omega)^n$. Then, there are terms in the average Hamiltonian (S15a) which vanish as Ω^{-1} and do not enter the lowest order of the expansion (cf. Eq. (3) of main text):

$$\bar{H}^{\mathrm{eff}(0)}_{\mathrm{Hub}} = VK_0 + (U_0-\Omega)\sum\nolimits_i (n_{i\uparrow}-\tfrac{1}{2})(n_{i\downarrow}-\tfrac{1}{2}). \tag{S17}$$

For the same reason, at first order only enter those terms which actually vanish as Ω^{-1} (cf. Eq. (4) of main text):

$$\bar{H}^{\mathrm{eff}(1)}_{\mathrm{Hub}} = (-i\mathcal{J}_1(\tfrac{\delta U}{\Omega})VK_+ + \mathrm{H.c.}) + \tfrac{V^2}{\Omega}(\mathcal{J}_0(\tfrac{\delta U}{\Omega}))^2[K_+,K_-]. \tag{S18}$$

Eq. (5) of main text

Here we calculate the commutator in Eq. (S18):

$$\begin{aligned}
[K_+,K_-] &= \sum_{ij\sigma}\sum_{kl\sigma'}[c^\dagger_{i\sigma}c_{j\sigma}n_{i\bar\sigma}\bar n_{j\bar\sigma}, c^\dagger_{k\sigma'}c_{l\sigma'}\bar n_{k\bar\sigma'}n_{l\bar\sigma'}]\\
&= \sum_{ij\sigma}\sum_{kl\sigma'}[c^\dagger_{i\sigma}c_{j\sigma}, c^\dagger_{k\sigma'}c_{l\sigma'}]n_{i\bar\sigma}\bar n_{j\bar\sigma}\bar n_{k\bar\sigma'}n_{l\bar\sigma'}\\
&+ \sum_{ij\sigma}\sum_{kl\sigma'}c^\dagger_{k\sigma'}c_{l\sigma'}[c^\dagger_{i\sigma}c_{j\sigma}, \bar n_{k\bar\sigma'}n_{l\bar\sigma'}]n_{i\bar\sigma}\bar n_{j\bar\sigma}\\
&+ \sum_{ij\sigma}\sum_{kl\sigma'}c^\dagger_{i\sigma}c_{j\sigma}[n_{i\bar\sigma}\bar n_{j\bar\sigma}, c^\dagger_{k\sigma'}c_{l\sigma'}]\bar n_{k\bar\sigma'}n_{l\bar\sigma'}.
\end{aligned} \tag{S19}$$

The commutators in Eq. (S19) give three- and two-site terms. If we retain only the two-site terms, then the first sum in Eq. (S19) reads:

$$\sum\nolimits_{ij}(n_{i\sigma}n_{i\bar\sigma}\bar n_{j\bar\sigma} - n_{j\sigma}n_{i\bar\sigma}\bar n_{j\bar\sigma}) = \sum\nolimits_{ij}(n_{i\sigma}-n_{j\sigma})n_{i\bar\sigma}\bar n_{j\bar\sigma}. \tag{S20}$$

Now, with the identitites $c_{i\sigma}n_{i\sigma} = c_{i\sigma}$ and $n_{i\sigma}c_{i\sigma} = 0$, together with their Hermitian conjugates, it is easy to see that terms in the second sum in Eq. (S19) are non-vanishing only if $\{i = l, j = k, \sigma' = \bar\sigma\}$, giving:

$$\begin{aligned}
&\sum\nolimits_{ij}c^\dagger_{j\sigma}c_{i\sigma}(-c^\dagger_{i\bar\sigma}c_{j\bar\sigma}n_{i\bar\sigma} - \bar n_{j\bar\sigma}c^\dagger_{i\bar\sigma}c_{j\bar\sigma})\\
&= \sum\nolimits_{ij}c^\dagger_{i\bar\sigma}c_{i\sigma}c^\dagger_{j\sigma}c_{j\bar\sigma}\\
&= \sum\nolimits_{ij}(c^\dagger_{i\uparrow}c_{i\downarrow}c^\dagger_{j\downarrow}c_{j\uparrow} + c^\dagger_{i\downarrow}c_{i\uparrow}c^\dagger_{j\uparrow}c_{j\downarrow})\\
&= \sum\nolimits_{ij}(S^+_iS^-_j + S^-_iS^+_j) = 2\sum\nolimits_{ij}(S^x_iS^x_j + S^y_iS^y_j).
\end{aligned} \tag{S21}$$

Analogously, terms in the third sum in Eq. (S19) are non-vanishing only if $\{i = k, j = l, \sigma' = \bar\sigma\}$, giving:

$$\begin{aligned}
&\sum\nolimits_{ij}c^\dagger_{i\sigma}c_{j\sigma}(n_{i\bar\sigma}c^\dagger_{i\bar\sigma}c_{j\bar\sigma} + c^\dagger_{i\bar\sigma}c_{j\bar\sigma}\bar n_{j\bar\sigma})\\
&= \sum\nolimits_{ij}c^\dagger_{i\sigma}c_{j\sigma}c^\dagger_{i\bar\sigma}c_{j\bar\sigma} = 2\sum\nolimits_{ij}c^\dagger_{i\uparrow}c^\dagger_{i\downarrow}c_{j\downarrow}c_{j\uparrow}.
\end{aligned} \tag{S22}$$

To proceed, we restrict ourselves to a subspace with double occupancy so large that we can neglect sinlgy occupied sites. In other words, we restrict ourselves to the local subspace $\{|0\rangle, |\uparrow\downarrow\rangle\}$. Within this subspace we have $n_{i\sigma} = n_{i\bar\sigma}$ so that Eq. (S20) simplifies to:

$$\sum\nolimits_{ij}n_{i\sigma}\bar n_{j\bar\sigma} = \sum\nolimits_{ij}n_{i\sigma}n_{i\bar\sigma}\bar n_{j\bar\sigma}\bar n_{j\sigma} = 2\sum\nolimits_{ij}n_{i\uparrow}n_{i\downarrow}\bar n_{j\downarrow}\bar n_{j\uparrow}. \tag{S23}$$

Moreover, within this subspace Eq. (S21) vanishes, so that the final result reads (cf. Eq. (5) of main text):

$$2\tfrac{V^2}{\Omega}(\mathcal{J}(\tfrac{\delta U}{\Omega}))^2\sum\nolimits_{ij}(c^\dagger_{i\uparrow}c^\dagger_{i\downarrow}c_{j\downarrow}c_{j\uparrow} + n_{i\uparrow}n_{i\downarrow}\bar n_{j\downarrow}\bar n_{j\uparrow}). \tag{S24}$$

This reproduces Eq.(2) of Ref. [41] for $\delta U = 0$, $\Omega = U_0$.

η-spin ferromagnetic Heisenberg

To recast Eq. (S24) to the ferromagnetic Heisenberg model considered in the main text, we carry out a transformation on the spin-down only:

$$c_{i\uparrow} \to \tilde c_{i\uparrow} = c_{i\uparrow}, \tag{S25}$$

$$c_{i\downarrow} \to \tilde c_{i\downarrow} = (-1)^i c^\dagger_{i\downarrow}. \tag{S26}$$

Here $(-1)^i = \pm 1$ on different sublattices of a bipartite lattice. Then the first term in Eq. (S24) transforms to:

$$\begin{aligned}
&-\sum\nolimits_{ij}(\tilde c^\dagger_{i\uparrow}\tilde c_{i\downarrow}\tilde c_{j\downarrow}\tilde c_{j\uparrow} + \tilde c^\dagger_{i\downarrow}\tilde c_{i\uparrow}\tilde c_{j\uparrow}\tilde c_{j\downarrow})\\
&= -\sum\nolimits_{ij}(\eta^+_i\eta^-_j + \eta^-_i\eta^+_j) = -2\sum\nolimits_{ij}(\eta^x_i\eta^x_j + \eta^y_i\eta^y_j).
\end{aligned} \tag{S27}$$

This has the same form of Eq. (S21) with the additional minus sign $(-1)^{i+j} = -1$ for nearest-neighbor sites. The η-spin has the same definition of the physical spin for the transformed electrons $\boldsymbol{\eta}_i = \frac{1}{2}\sum_{\alpha\beta}\tilde c^\dagger_{i\alpha}\boldsymbol{\sigma}_{\alpha\beta}\tilde c_{i\beta}$ where $\boldsymbol{\sigma}$ is the vector of the three Pauli matrices:

$$\begin{aligned}
\eta^x_i &= \frac{\tilde c^\dagger_{i\uparrow}\tilde c_{i\downarrow} + \tilde c^\dagger_{i\downarrow}\tilde c_{i\uparrow}}{2},\\
\eta^y_i &= \frac{\tilde c^\dagger_{i\uparrow}\tilde c_{i\downarrow} - \tilde c^\dagger_{i\downarrow}\tilde c_{i\uparrow}}{2i},\\
\eta^z_i &= \frac{\tilde c^\dagger_{i\uparrow}\tilde c_{i\uparrow} - \tilde c^\dagger_{i\downarrow}\tilde c_{i\downarrow}}{2}.
\end{aligned} \tag{S28}$$

Additionally, if one defines $\eta^+_i = \tilde c^\dagger_{i\uparrow}\tilde c_{i\downarrow}$ and $\eta^-_i = \tilde c^\dagger_{i\downarrow}\tilde c_{i\uparrow}$ then $\eta^x_i = (\eta^+_i + \eta^-_i)/2$ and $\eta^y_i = (\eta^+_i - \eta^-_i)/2$.

To consider the second term in Eq. (S24), we notice that under the transformation (S25) the density operator transforms as $n_{i\uparrow} \to \tilde n_{i\uparrow} = n_{i\uparrow}$ and $n_{i\downarrow} \to \tilde n_{i\downarrow} = 1 - n_{i\downarrow}$. Then, this term transforms to (keep in mind that in the considered subspace $n_{i\sigma} = n_{i\bar\sigma}$):

$$\sum\nolimits_{ij}\tilde n_{i\bar\sigma}\tilde n_{j\sigma} = \sum\nolimits_{ij}(\tilde n_{i\uparrow}\tilde n_{j\downarrow} + \tilde n_{i\downarrow}\tilde n_{j\uparrow}) = -2\sum\nolimits_{ij}(\eta^z_i\eta^z_j - \tfrac{1}{4}). \tag{S29}$$

The last equality is best demonstrated veryfing that the operators have the same matrix elements in the considered subspace. Alternatively, an explicit derivation reads:

$$\begin{aligned}
&\tilde n_{i\uparrow}\tilde n_{j\downarrow} + \tilde n_{i\downarrow}\tilde n_{j\uparrow}\\
&= \tfrac{1}{2}(\tilde n_{i\uparrow}\tilde n_{j\downarrow} + \tilde n_{i\downarrow}\tilde n_{j\uparrow}) + \tfrac{1}{2}(\tilde n_{i\uparrow}\tilde n_{j\downarrow} + \tilde n_{i\downarrow}\tilde n_{j\uparrow})\\
&= \tfrac{1}{2}(\tilde n_{i\uparrow}\tilde n_{j\downarrow} + \tilde n_{i\downarrow}\tilde n_{j\uparrow}) + \tfrac{1}{2}(\tilde n_{i\uparrow}(1-\tilde n_{j\uparrow}) + \tilde n_{i\downarrow}(1-\tilde n_{j\downarrow}))\\
&= -2(\tfrac{1}{4}(\tilde n_{i\uparrow}-\tilde n_{i\downarrow})(\tilde n_{j\uparrow}-\tilde n_{j\downarrow}) - \tfrac{1}{4}).
\end{aligned}$$

Here it is crucial the use of $\tilde n_{i\uparrow} + \tilde n_{i\downarrow} = 1$.